JCTC Journal of Chemical Theory and Computation

Article

pubs.acs.org/JCTC

Ab Initio Extension of the AMOEBA Polarizable Force Field to Fe^{2+}

David Semrouni,[†] William C. Isley, III,[†] Carine Clavaguéra,[‡] Jean-Pierre Dognon,[§] Christopher J. Cramer,[†,*] and Laura Gagliardi[†,*]

[†]Department of Chemistry, Chemical Theory Center, and Supercomputing Institute, University of Minnesota, 207 Pleasant St. SE, Minneapolis, Minnesota 55455, United States

[‡]Laboratoire des Mécanismes Réactionnels, Département de Chimie, École Polytechnique, CNRS, 91128 Palaiseau Cedex, France

[§]CEA/Saclay, UMR 3299 CEA/CNRS SIS2M, Laboratoire de Chimie de Coordination des Eléments f, F-91191 Gif-sur-Yvette, France

Supporting Information

ABSTRACT: We extend the AMOEBA polarizable molecular mechanics force field to the Fe^{2+} cation in its singlet, triplet, and quintet spin states. Required parameters are obtained either directly from first principles calculations or optimized so as to reproduce corresponding interaction energy components in a hexaaquo environment derived from quantum mechanical energy decomposition analyses. We assess the importance of the damping of point-dipole polarization at short distance as well as the influence of charge-transfer for metal-water interactions in hydrated Fe^{2+}; this analysis informs the selection of model systems employed for parametrization. We validate our final Fe^{2+} model through comparison of molecular dynamics (MD) simulations to available experimental data for aqueous ferrous ion in its quintet electronic ground state.

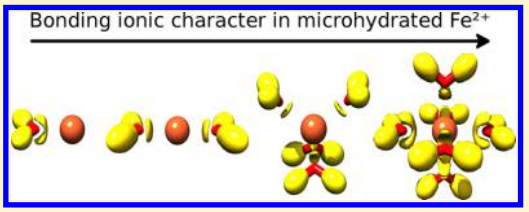

I. INTRODUCTION

Metal cations are of fundamental importance in biophysical systems where they can play either a structural role (e.g., zinc fingers,[1] or helix−loop−helix domains such as Ca^{2+} EF hands[2,3]) or a functional one (e.g., nitrogen fixation,[4] oxygen transport,[5] or electron transfer[6]). Iron is the central element in heme proteins, and it has recently been suggested[7] that, in early stages of life on Earth, ferrous ion (Fe^{2+}) fulfilled many additional functions, including, for example, those nowadays filled by Mg^{2+} in RNA folding. In addition to its many biological roles, Fe^{2+} is widely employed in catalysis and as a templating ion for the formation of metal−organic frameworks[8] and cages.[9,10] These various phenomena provide substantial motivation to accurately model the solvation and cation−ligand interactions of Fe^{2+}, especially with respect to the applicability and improvement of both molecular mechanical (force field) and quantum mechanical methods,[11−17] successfully used for the study of the solvation of other cations.[18−20]

Classical force fields typically treat intermolecular interactions as sums of pairwise van der Waals and electrostatic terms. In force fields that do not explicitly include electric polarization, many-body interactions are taken into account only implicitly, viz., through parametrization of nonbonded interactions against experimental or high-level quantum chemical data. However, the inclusion of an explicit polarization term in the potential energy expression constitutes an improvement in the term-by-term physicality for classical force fields. Moreover, as the polarizing character of a cation increases with increasing charge density, it has been found that quantitative treatments of solvation energetics for systems including cations having charges of 2 or higher essentially *require* inclusion of a polarization term.[21] The importance of polarization has also been noted for the modeling of protein binding sites.[22,23]

Electric polarization is defined as the response of a molecule to an external electric field. This response consists of the interconnected distortion of the electron density and the relaxation of the atomic nuclear positions (i.e., the molecular geometry). With a nonpolarizable force field, molecular deformation in the presence of an electric field is approximated through interaction of the field with the fixed charge distribution of the molecule, but additional effects associated with induction of the electronic density are not included. In this work, we will, in certain instances, assess "static polarization", which we define as the redistribution of the electronic density in response to the presence of an electric field for a molecular structure, the geometry of which is held frozen.

Polarization effects have been included in molecular mechanical models in various ways.[24] The AMOEBA force field[25−27] implements a point-dipole polarization model. Applequist induced-point-dipole models[28] are subject to the risk of "polarization catastrophe", that is, the nonconvergence of the polarization energy between two atoms at short distance. Tholé discussed this issue and introduced a damping factor[29] to avoid this divergence at short-range; the Tholé model has several variations.[30] The AMOEBA force field uses a damping scheme similar to the smearing of charges in the Tholé

Received: March 25, 2013
Published: June 5, 2013

   dx.doi.org/10.1021/ct400237r | J. Chem. Theory Comput. 2013, 9, 3062−3071

approach.[29] The AMOEBA force field considers atomic multipoles up to quadrupoles and dipole polarizabilities and includes many-body effects through self-consistent computation of mutually induced dipoles.

The ferrous ion has the electronic configuration [Ar] $3d^6$; this valence configuration permits three different spin multiplicities: singlet, triplet and quintet, the relative energies of which depend on environment. In preceding work, Swart et al.[31] have described a polarizable force field for Fe^{2+} covalently bonded to two trispyrazolylborate ligands (Tp). Using quantum chemical data, they obtained two force field parameter sets to model the spin crossover between the singlet and the quintet spin states of Fe(II)$(Tp)_2$. As the metal is defined to be covalently bonded to its ligands, parameters associated with the different spin states are different not only for the metal but also for the surrounding atoms, in terms of both noncovalent and covalent interactions.

In the present work, we develop a general polarizable force field for the bare Fe^{2+} cation designed for use in the *absence* of explicit metal−ligand bonding definitions; that is, all Fe^{2+} interactions are defined to be nonbonded. In particular, we parametrize the singlet, triplet, and quintet spin states for the cation in an aqueous environment. Features of the Fe^{2+}−water interactions are determined both by topological analysis of the electron localization function[32] (ELF) and energy decomposition analysis at the second-order Møller−Plesset level of theory, permitting increased physicality in the parametrization of the force field term-by-term. Study of the covalency of the iron−water interactions as a function of the number of water molecules is also used to rationalize the choice of the optimal system to be considered for force field parametrization. In the remainder of this article, section II describes the determination of the atomic polarizability of Fe^{2+}, the computation of gas-phase reference energies, and energy decomposition analysis. In section III, we assess the nature of iron−water interactions for microhydrated Fe^{2+} models and define the system we use in force field parameter optimization. Section IV addresses force field validation, and Section V provides conclusions.

II. COMPUTATIONAL DETAILS

II.1. Ab Initio Atomic Polarizabilities. AMOEBA uses atomic point-dipole polarizabilities to compute induced dipoles on atoms in response to a static electric field. We determined static electric dipole polarizabilities at the second-order Møller−Plesset perturbation (MP2) level of theory with a fully uncontracted aug-cc-pVQZ[33] basis set (large, uncontracted basis sets are generally required for the computation of accurate dipole polarizabilities[34,35]) employing the MOLPRO 2010.1 program package.[36] In particular, we performed numerical differentiation of finite-field dependent energies.

For an atom, the static dipole polarizability α_D is defined as[37,38]

$$\alpha_D = -\left\{\frac{\partial^2 E(\vec{f})}{\partial f_\mu \partial f_\mu}\right\}_{f=0} \quad (1)$$

where $E(\vec{f})$ is the total electronic energy as a function of the electric field $\vec{f}$ and differentiation is independent of the choice of spatial coordinate μ. We computed $E(\vec{f})$ for a field strength of 0.005 au, which value is small enough to exclude hyperpolarizability effects but large enough to avoid noise errors in numerical differentiation. From these calculations, the dipole polarizabilities of Fe^{2+} in its singlet, triplet, and quintet states are 0.547, 0.549, and 0.550 $Å^3$, respectively. The negligible variation in these values as a function of spin state is responsible for interaction energy curves that are largely independent of spin state at Fe^{2+}−X distances larger than 3 Å for a given partner X, as described later for the specific case of $[Fe(H_2O)_5]^{2+}$−H_2O. Atomic polarizabilties were rounded to the hundredths of $Å^3$, as done recently by Xiang and Ponder for Zn^{2+} and Cu^{2+}, leading to a common value of 0.55 $Å^3$ for the three spin states of Fe^{2+}.[16]

II.2. Ab Initio Reference Energies. Interaction energies were computed between $[Fe(H_2O)_5]^{2+}$ clusters and H_2O for singlet, triplet, and quintet spin multiplicities. First, the structure of the hexa-hydrated system, $[Fe(H_2O)_6]^{2+}$, was optimized for each spin multiplicity at the M06-L[39] level of density functional theory (benchmarking studies have established the good performance of the M06-L functional in systems containing transition metals)[40,41] using the Stuttgart [8s7p6d1f | 6s5p3d1f] ECP10MDF contracted pseudopotential basis set[42] for Fe, and the 6-31G(d) basis set for H and O. Optimization employed an ultrafine integration grid. Next, starting from the optimized geometry for each spin state, a dissociation path was generated by displacing one water molecule along its Fe−O vector, while holding the remaining geometric degrees of freedom of $[Fe(H_2O)_5]^{2+}$ and H_2O fixed. Along each of these three spin-state specific paths, interaction energies were computed for *all* spin multiplicities at the MP2 level of theory, using the Stuttgart [8s7p6d1f | 6s5p3d1f] ECP10MDF contracted pseudopotential basis set on Fe and the def2-TZVP basis set[43] on all other atoms. Integral evaluations made use of the W06 density fitting basis set of Ahlrichs and co-workers[43,44] within the resolution of the identity approximation to speed up the evaluation of Coulomb integrals. For each of these single point calculations, counterpoise corrections[45] were included to address basis set superposition error (BSSE). All of these calculations were accomplished with the Gaussian 09 program suite.[46] (See the Supporting Information.)

In order to assess the possible importance of multideterminantal character in the various wave functions, we also computed large basis set CASPT2[47] relative energies for select points along the various curves, but the differences from the single reference MP2 relative energies were found to be small in all instances. Evidently multireference effects are unimportant for $[Fe(H_2O)_5]^{2+}$−H_2O. The CASPT2 calculations show an electronic structure dominated by a single electronic configuration (see the Supporting Information).

II.3. Energy Decomposition Analysis. For our $[Fe(H_2O)_n]^{2+}$ systems, we computed interaction energies between $[Fe(H_2O)_{n-1}]^{2+}$ and H_2O, as well as between bare Fe^{2+} and $(H_2O)_n$ clusters. The nature of the intercluster interactions in microhydrated Fe^{2+}, and, in particular, the many-body interactions, was studied using the localized molecular orbital energy decomposition analysis (LMOEDA) method[48,49] at the MP2 level of theory with a cc-pVTZ basis set.[33,50] All calculations were performed with the quantum chemistry program package GAMESS-US (2012-R1 version).[51] In LMOEDA, the total interaction energy ΔE_{int} is decomposed into five terms: electrostatic (ΔE_{es}), exchange (ΔE_{ex}), repulsion (ΔE_{rep}), polarization (ΔE_{pol}), and dispersion (ΔE_{disp}):

$$\Delta E_{int} = \Delta E_{es} + \Delta E_{ex} + \Delta E_{rep} + \Delta E_{pol} + \Delta E_{disp} \quad (2)$$

At the MP2 level of theory, the dispersion term in LMOEDA is the MP2 correction to the Hartree−Fock interaction energy ΔE_{int}, and all the interaction terms are corrected for BSSE.

II.4. AMOEBA Force Field. *II.4.1. General Description.* We have parametrized Fe^{2+} in a manner to be consistent with the AMOEBA force field in the *absence* of other than nonbonded terms. The nonbonded intermolecular potential of AMOEBA can be decomposed as the sum of three terms:

$$\Delta E_{int} = \Delta E_{vdW} + \Delta E_{es} + \Delta E_{pol} \tag{3}$$

where E_{vdW} and E_{es} are pairwise potentials defining the van der Waals (vdW) and the electrostatic energy contributions, respectively. The van der Waals term takes into account exchange-repulsion and dispersion interactions, while the electrostatic term results from the interaction of atomic permanent multipoles from charges up to quadrupoles. The polarization component of the energy, E_{pol} is a nonadditive term computed accounting for mutual, self-consistent induction of atomic sites.

II.4.2. Repulsion-Dispersion. Repulsion and dispersion are accounted for in AMOEBA using Halgren's buffered 14−7 potential:[52]

$$E_{vdW}^{ij} = \varepsilon_{ij}\left(\frac{1+\delta}{\frac{R_{ij}}{R_{ij}^0}+\delta}\right)^7\left(\frac{1+\gamma}{\left(\frac{R_{ij}}{R_{ij}^0}\right)^7+\gamma}-2\right) \tag{4}$$

where ε_{ij} is the potential well depth, R_{ij} is the separation distance, R_{ij}^0 is the minimum energy distance, and δ and γ are buffering constants respectively set to 0.07 and 0.12 by Halgren. As is true for many other classical force fields, AMOEBA uses mixing rules to compute pairwise interactions from atomic van der Waals parameters, thereby avoiding the introduction of pair parameters. The mixing rules used in AMOEBA are

$$\varepsilon_{ij} = \frac{4\varepsilon_{ii}\varepsilon_{jj}}{(\varepsilon_{ii}^{1/2}+\varepsilon_{jj}^{1/2})^2} \tag{5}$$

and

$$R_{ij}^0 = \frac{(R_{ii}^0)^3+(R_{jj}^0)^3}{(R_{ii}^0)^2+(R_{jj}^0)^2} \tag{6}$$

Note that van der Waals atomic sites for hydrogen atoms are displaced toward the atom to which they are attached according to a specific AMOEBA scheme.[27]

II.5. Molecular Mechanics Computations and Molecular Dynamics Simulations. The Tinker package version 6.0[53] was used for all molecular mechanics calculations, all of which involved the (extended) AMOEBA force field.[25−27] In particular, the AMOEBA water model is described in ref 26.

II.5.1. Molecular Dynamics Simulations. Equations of motion were integrated according to the modified Beeman algorithm[54] implemented in Tinker, using a time step of 1 fs. Structures were saved for analysis every 100 steps (0.1 ps). Temperature was maintained at 298 K using a Berendsen thermostat[55] and a bath coupling time of 0.1 ps, as previously used for hydration of other cations.[11,56−58] Though the Berendsen weak coupling method does not reproduce any standard thermodynamic ensemble, the ensemble it generates is between the canonical and the microcanonical ensembles.[59] When periodic boundary conditions (PBC) were applied, long-range electrostatics were computed using particle-mesh Ewald summation of atomic multipoles up to order 5 and a cutoff of 7 Å in real space. A cutoff radius of 10 Å was employed for vdW interactions. Equilibration periods of 50 ps were followed by production trajectories of 2 ns, from which radial distribution functions (RDFs) were computed. Additional details are included as part of the discussion.

II.5.2. Free Energy Calculations. Free energy perturbation (FEP) molecular dynamics calculations in the canonical ensemble (NVT) were undertaken in order to evaluate the solvation free energy of ground-state quintet Fe^{2+} in water. These calculations involved a pre-equilibrated cubic simulation box containing 1 Fe^{2+} cation and 511 water molecules with a fixed edge length of 24.857 Å. Simulations were propagated for 500 ps/window (this procedure has been used previously for other cations, cf. refs 11 and 57). The Bennett acceptance ratio[60] was used to compute the Helmholtz free energy difference, ΔA between two successive perturbation states λ_i and λ_{i+1}:

$$\Delta A_{\lambda_i \mapsto \lambda_{i+1}} = RT\ln\frac{\sum_j^{\lambda_i}\frac{1}{f(U(j,\lambda_{i+1})-U(j,\lambda_i)-C)}}{\sum_{j'}^{\lambda_{i+1}}\frac{1}{f(U(j',\lambda_i)-U(j',\lambda_{i+1})+C)}}+C \tag{7}$$

where the function f is the Fermi function:

$$f(x) = \frac{1}{1+e^{x/RT}} \tag{8}$$

with R the universal gas constant and T temperature, and where the sums in eq 7 are acquired over configurations j and j' sampled during the MD trajectories associated with λ_i and λ_{i+1}, respectively. $U(j,\lambda_{i+1})$ is the energy of configuration j evaluated with the shift parameter λ_{i+1} and $U(j',\lambda_1)$ is defined analogously. C is a shift constant used to estimate ΔA through self-consistent adjustment. This guess, C, is set to the current estimate of ΔA at each step of this self-consistent procedure, until convergence of $C = \Delta A$.

FEP calculations proceeded first with introduction of vdW interactions followed by electrostatic interactions. For the vdW interactions, 14 FEP steps were simulated for λ values of 0.0, 0.0001, 0.001, 0.01, 0.1, 0.2, 0.3, 0.4, 0,5, 0.6, 0.7, 0.8, 0.9, and 1.0. For each step λ of the perturbation, the vdW radius of the cation was defined by

$$R_{Fe^{2+}}(\lambda) = \lambda R_{Fe^{2+}}^0 \tag{9}$$

and the associated vdW well depth was taken to be

$$\varepsilon_{Fe^{2+}}(\lambda') = \lambda'\varepsilon_{Fe^{2+}}^0 \tag{10}$$

Subsequently, 41 more FEP steps were carried out growing both the charge and atomic polarizability of the cation. These steps propagated the parameter λ' from 0 to 1 with an increment of 0.025, scaling the charge and polarizability of the cation linearly. In all perturbation steps, after taking the 50 first ps of each trajectory as an equilibration phase, the remaining 450 ps were used for free energy calculations. For each window of perturbation, the free energy was recomputed using the last 300 ps of the same simulations (i.e., treating the first 200 ps as equilibration time, instead of only the first 50 ps) to verify the sufficiency of both the equilibration phase time length and the sampling of the phase space obtained during the production phase.

III. PARAMETERIZATION OF Fe^{2+} FOR AMOEBA

III.1. Nature of the Metal−Water Interaction. Topological analysis of the electron density using the electron localization function[32] (ELF) was undertaken for the three spin multiplicities of the microhydrated complexes $[Fe(H_2O)_n]^{2+}$ with n ranging from 1 to 6 (the DGrid 4.6 program package[61] was used for ELF analysis of Gaussian 09 densities). For microhydration with water molecules up to the tetrahydrated complex, the metal−water interaction is characterized by a substantial degree of covalency (see Figure 1 for the quintet

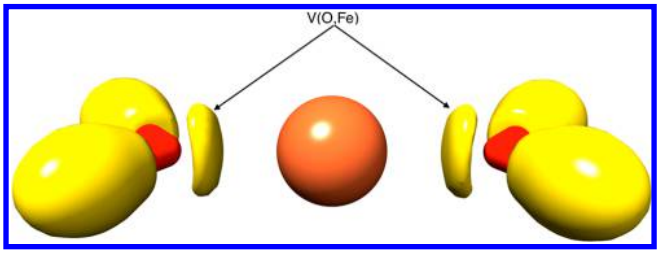

Figure 1. ELF basins of quintet $[Fe(H_2O)_2]^{2+}$ complex. The valence basin V(O,Fe) corresponds to electron sharing between O and Fe (bonding region) and finds its origin in a charge transfer interaction.

spin state), and indeed, the Fe^{2+}−water interaction is predicted to be more covalent than the Zn^{2+}−water interaction in such instances.[57] However, this contribution of covalency to the overall interaction decreases with each additional water ligand. Indeed, the shape of the oxygen ELF basins V(O) calculated for the quintet spin state of $[Fe(H_2O)_6]^{2+}$ (Figure 2), shows their

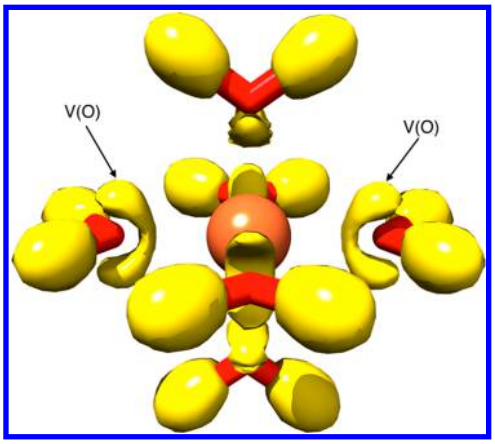

Figure 2. ELF basins for the quintet $[Fe(H_2O)_6]^{2+}$ complex. No bonding region O−Fe was identified. The valence basins V(O) correspond to the oxygen lone pairs.

noncovalent lone pair nature and a complete absence of covalent Fe−O character. With this in mind, we elected to optimize our Fe^{2+} parameters based on a hexacoordinated system so as to avoid charge-transfer effects relevant for minimally ligated compounds but *not* likely to be relevant to condensed phase phenomena.

We note that metal cation parametrizations have recently been performed for tetra- and hexahydrated complexes of Cu^{2+} and Zn^{2+} using both the standard and a valence-bond extended versions of the AMOEBA force field.[16] The potentials based on valence bond theory include a formal bonding term, accounting for the partially covalent nature of metal−ligand interactions, as well as angular terms penalizing the energy of some spatial conformations. With such terms included, the force field can accurately represent Jahn−Teller distorsions and, for example, predict square planar coordination of Cu^{2+} rather than tetrahedral. Given the context of the weak ligand field of aquo substituents, however, we opt here for the simplicity of purely nonbonded interaction potentials for iron, anticipating that these will be useful starting points for ongoing parametrizations involving other ligating atoms.

III.2. Polarization Parameters. *III.2.1. Dipole Polarizability.* In AMOEBA, a point dipole on atom i is induced by the total electric field at the nuclear position. The electric field is determined from the distributed permanent multipoles M_j of other atoms j as well as their induced dipoles (using Stone notation[62]) according to

$$\mu_{i,\alpha}^{\mathrm{ind}} = \alpha_i\{\sum_j [T_\alpha^{ij} q_j + \sum_\beta (T_{\alpha\beta}^{ij}\mu_{j,\beta} + \sum_\gamma (T_{\alpha\beta\gamma}^{ij}\theta_{j,\beta\gamma}))] + \sum_{j'} T_{\alpha\beta}^{ij'}\mu_{j',\beta}^{\mathrm{ind}}\} \quad (11)$$

for $\alpha,\beta,\gamma = x,y,z$ and where α_i is the isotropic polarizability of atom i, T^{ij} is the interaction matrix of the polarizability with the charge q_j, dipole μ_j, and quadrupole θ_j of atom j, as defined in eqs 12, 13, and 14, respectively, and R is the distance vector between atoms i and j. Permanent multipoles are summed on j, while μ_j^{ind} is the dipole induced on atom j by the total electric field at *that* position.

$$T_\alpha^{ij} = -\frac{R_\alpha}{R^3} \quad (12)$$

$$T_{\alpha\beta}^{ij} = -\frac{\delta_{\alpha\beta}}{R^3} + \frac{3R_\alpha R_\beta}{R^5} \quad (13)$$

$$T_{\alpha\beta\gamma}^{ij} = -\frac{3(R_\alpha\delta_{\beta\gamma} + R_\beta\delta_{\alpha\gamma} + R_\gamma\delta_{\alpha\beta})}{R^5} - \frac{15R_\alpha R_\beta R_\gamma}{R^7} \quad (14)$$

As noted, α_i is 0.55 Å^3 for all three spin states of Fe^{2+}. The induced dipoles μ_i^{ind} are calculated first from the polarization due to the electric field of the permanent atomic multipole distribution (direct polarization). The induced dipoles modify the total electric field so that further iterations are required in order to achieve self-consistent convergence (mutual polarization).

To avoid the so-called polarization catastrophe associated with interactions at short distances, the polarization interaction is damped as proposed by Tholé,[29] but using an exponential smearing function:

$$\rho = \frac{3a}{4\pi} e^{-au^3} \quad (15)$$

where the effective distance u between two interacting sites i and j is defined as $u = r_{ij}/(\alpha_i\alpha_j)^{1/6}$ where r_{ij} is the interatomic separation, α_i and α_j are the respective atomic dipole polarizabilities, and a is a unitless parameter characterizing the width of the charge smearing to be used in the Tholé damping model. Thus, a may be referred to as the damping parameter and ρ as the smeared charge density. Resulting damped interaction tensors are determined from eqs 16, 17, and 18.

$$T_\alpha^{ij} = -(1 - e^{-au^3})\frac{R_\alpha}{R^3} \quad (16)$$

$$T^{ij}_{\alpha\beta} = -(1 - e^{-au^3})\frac{\delta_{\alpha\beta}}{R^3} + [1 - (1 + au^3)e^{-au^3}]\frac{3R_\alpha R_\beta}{R^5} \quad (17)$$

$$T^{ij}_{\alpha\beta\gamma} = [1 - (1 + au^3)e^{-au^3}]\frac{3(R_\alpha\delta_{\beta\gamma} + R_\beta\delta_{\alpha\gamma} + R_\gamma\delta_{\alpha\beta})}{R^5} - \left[1 - \left(1 + au^3 + \frac{3}{5}a^2u^6\right)e^{-au^3}\right]\frac{15R_\alpha R_\beta R_\gamma}{R^7} \quad (18)$$

In all our calculations, we converged the AMOEBA induced atomic dipoles to 10^{-6} D. The iterative procedure was accelerated using a successive over-relaxation technique[63] (SOR) with a SOR convergence acceleration factor of 0.75.

III.2.2. Damping Factor Optimization. By default, AMOEBA uses a standard polarization damping factor $a = 0.39$, this value having been optimized for atoms in molecules and singly charged ions.[26] However, this damping factor has generally been adjusted to other values for doubly charged cations added to the AMOEBA force field, for example, for Mg^{2+}, Ca^{2+}, and Zn^{2+}.[57,64] Recently, AMOEBA parameters for Th^{4+} have also been reported and validated for modeling aqueous solutions of this actinide.[11]

Using the ion polarizability α computed as described, we found that a value of 0.113 for a led to AMOEBA polarization energies optimally in agreement with the MP2 LMOEDA polarization terms computed for separation distances of 3 Å or larger for each spin state of hexacoordinated $[Fe(H_2O)_5]^{2+}-(H_2O)$. At smaller distances, charge-transfer effects contribute significantly to the LMOEDA polarization component, and in the absence of a specific force-field charge-transfer term (which we do not include), the resulting energy changes associated with charge-transfer are more properly handled in the fitting of the van der Waals component of the energy, as described later.

Our value of 0.113 for the damping parameter a is close to the value of 0.16 recently employed for both Zn^{2+} and Cu^{2+} by Xiang and Ponder.[16] Indeed, the prior parametrizations of zinc illustrate an important point. In the more recent work of Xiang and Ponder, the damping factor was chosen from analysis of tetra- and hexaaquo complexes of the metal. In earlier work, however, parametrization was based on Zn^{2+} interacting with only a single water molecule, from which a damping parameter of 0.2096 was derived.[57] The latter model has been successfully employed in aqueous[57] and biological[65] environments. However, the parametrization may have suffered from charge transfer effects owing to the low coordination of the metal cation, with the damping parameter taking on an unphysical value in an attempt to compensate. For simulations in bulk solution, metal ions will generally be surrounded by most or all of their first solvation shell and that is why we chose $Fe^{2+}(H_2O)_5-(H_2O)$ as the more physical model to employ for optimizing a for Fe^{2+}.

III.3. Parameterization of the Repulsion-Dispersion Term. We note again that we generated sets of structures for three different dissociation curves, deriving from the $Fe^{2+}(H_2O)_6$ clusters optimized individually for each spin state. The van der Waals parameters appearing in eqs 4, 5, and 6 were optimized for each spin state of Fe^{2+} by least-squares minimization against MP2 reference energies for structures on the curve originally generated for that same spin state (Table 1). As expected based on d orbital occupation numbers, the singlet state of Fe^{2+} is found to have the smallest vdW radius parameter of 2.055 Å, while those for the triplet and quintet states are substantially larger at 3.762 and 2.798 Å, respectively. The early onset of repulsion that occurs with the larger radii predicted for the higher spin states is consistent with the shallow minima predicted for these states at the MP2 level compared to the more attractive potential predicted for the singlet state.

Table 1. AMOEBA vdW Parameters Optimized for Fe^{2+}

spin multiplicity	R^0_{Fe2+} (Å)	ε^0_{Fe2+} (kcal/mol)
singlet	2.055	0.187
triplet	3.762	0.033
quintet	2.798	0.390

Figures 3, 4, and 5 provide the BSSE-corrected reference MP2 energies, as well as the AMOEBA interfragment interaction energy curves, for *all* spin states computed along the singlet, triplet, and quintet dissociation paths, respectively (the asymptote for all curves is taken to be zero; i.e., the curves are not asymptotically separated by the state-energy splittings for $Fe^{2+}(H_2O)_5$). For the singlet state, the minimum interaction energy is observed at 2.05 Å for both the MP2 and AMOEBA calculations. The interaction energy at the minimum is predicted to be −31.9 kcal/mol at the AMOEBA level and −32.9 kcal/mol at the MP2 level (Figure 3). For the other spin states *evaluated for the singlet minimum energy geometry*, the AMOEBA interaction energies are predicted to be too large by about 4 kcal/mol compared to the MP2 results, although the shapes of the AMOEBA potential energy curves are otherwise quite similar to the MP2 references. Thus, the shorter Fe−O bond distances associated with the singlet geometries (about 0.12 Å compared to the higher spin states) are predicted to introduce less destabilization at the force field level than at the ab initio level. While this agreement is only fair, it must be borne in mind that the geometries in question are quite high in energy compared to the respective triplet and quintet optimized species. Indeed, those structures on the singlet path that have the lowest energies for the triplet and quintet states, and which are thus *lower* than the triplet or quintet energies predicted for the singlet minimum, are still predicted to be 9.0 and 14.5 kcal/mol above the fully optimized triplet and quintet minima, respectively, so such structures would generally not be important in equilibrium simulations in any case.

Considering Figures 4 and 5 in more detail, we find that the triplet and quintet geometries are sufficiently similar that the agreement between AMOEBA and MP2 is quite good along the dissociation pathways for both states; the root-mean-square deviation over all energies is within 0.24 kcal/mol or better and, indeed, generally to within 0.15 kcal/mol. Singlet interaction energies at the AMOEBA level are predicted to be up to 1 kcal/mol smaller than corresponding MP2 values near the potential minimum. Thus, the stretched Fe−O distances for the triplet and quintet $Fe^{2+}(H_2O)_5$ structures compared to the singlet structure are predicted to lead to somewhat more destabilization at the force field level than the ab initio. Again, we emphasize that these geometries are far from singlet equilibrium structures, so reduced force field accuracy on those structures is to be expected.

IV. VALIDATION OF Fe^{2+} FORCE FIELD PARAMETERS

Comparing to the MP2 dissociation curves for all spin states as described is a necessary first step in evaluating our force field extension. To further validate the new Fe^{2+} parameters, we examined relaxation of the geometric constraints in the

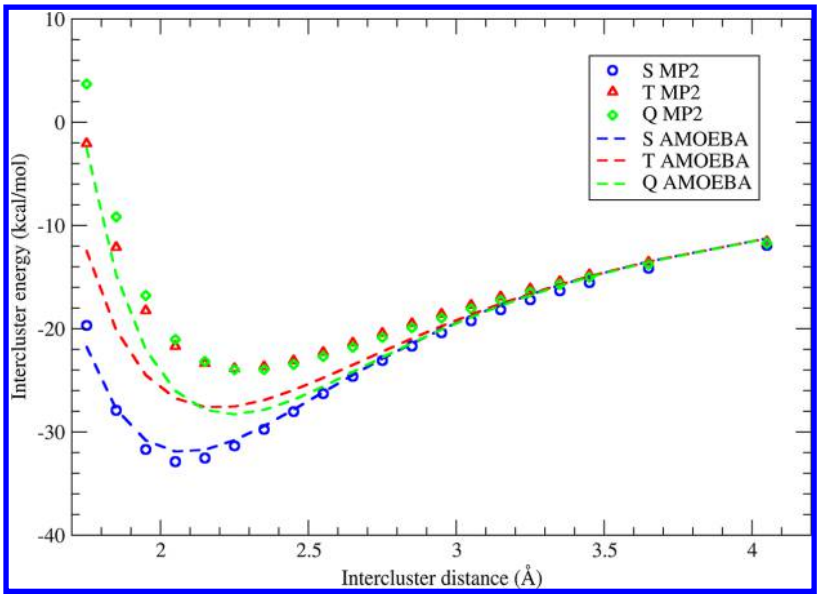

Figure 3. $[Fe(H_2O)_5]^{2+}$–H_2O dissociation profiles for the singlet, triplet, and quintet spin states along the singlet dissociation path.

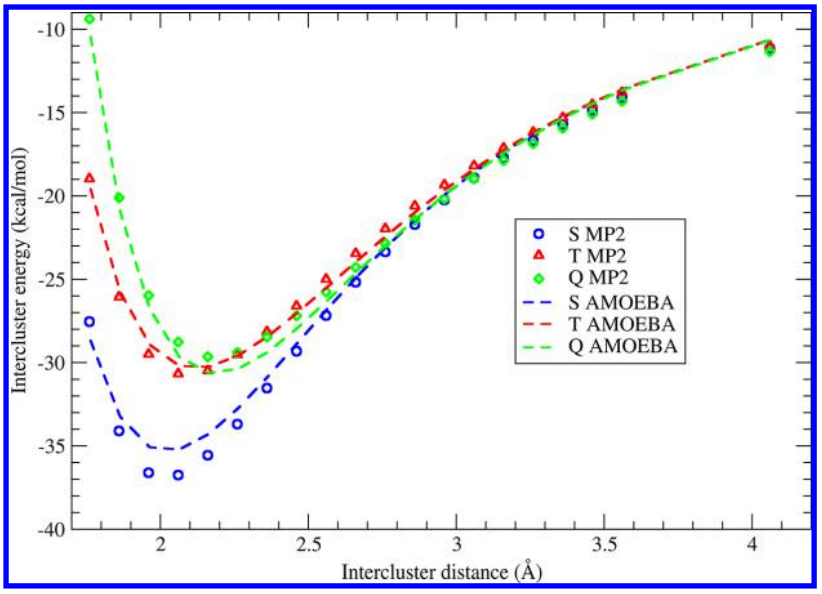

Figure 4. $[Fe(H_2O)_5]^{2+}$–H_2O dissociation profiles for the singlet, triplet, and quintet spin states along the triplet dissociation path.

hexaaquo structures, and we also performed classical simulations of Fe^{2+} in water in order to compare both structural and energetic properties with available experimental data[66−71] gathered in reviews refs 72 and 73 and with other simulations reported in the literature.[74,75] As experimental aqueous Fe^{2+} data are available only for its quintet ground state, our bulk simulations were performed for that state (methodological details are in section II.5).

IV.1. Structural Properties of Gas-Phase $Fe^{2+}(H_2O)_6$. For each spin state, we optimized the structure of $Fe^{2+}(H_2O)_6$ with its corresponding AMOEBA parameters. All structures were found to have D_{2h} symmetry with three unique Fe−O distances (Table 2). For the singlet state, the AMOEBA Fe−O distances range from 2.023 to 2.048 Å while the M06-L values range from 2.032 to 2.075 Å. The (ground-state) quintet structure has the longest Fe−O distances, as might be expected given at least single occupation of every d orbital. AMOEBA predicts Fe−O bond lengths of 2.159 to 2.192 Å, and the M06-L values are similar, ranging from 2.118 to 2.174 Å. At the density functional level, a strong Jahn−Teller distortion is predicted for the triplet structure, with one unique Fe−O bond length being more than 0.1 Å longer than the others. In the absence of valence bond terms, our AMOEBA extension cannot reproduce this distortion, although the AMOEBA Fe−O distances for the triplet state are all within the range predicted at the M06-L level.

IV.2. Bulk solvation of Fe^{2+}. We next consider the dynamical behavior of Fe^{2+} in the presence of large numbers of water molecules, extending to bulk solvation. In particular, we examine Fe^{2+} in a spherical cluster containing 216 H_2O molecules bounded by a repulsive wall potential at 14 Å from the cation; three separate trajectories were propagated for this system, as described in Section II.5.1, and results are reported here averaged over all three trajectories. We also studied the cation in a cubic box containing 511 water molecules with an edge length of 24.857 Å subject to periodic boundary

dx.doi.org/10.1021/ct400237r | J. Chem. Theory Comput. 2013, 9, 3062−3071

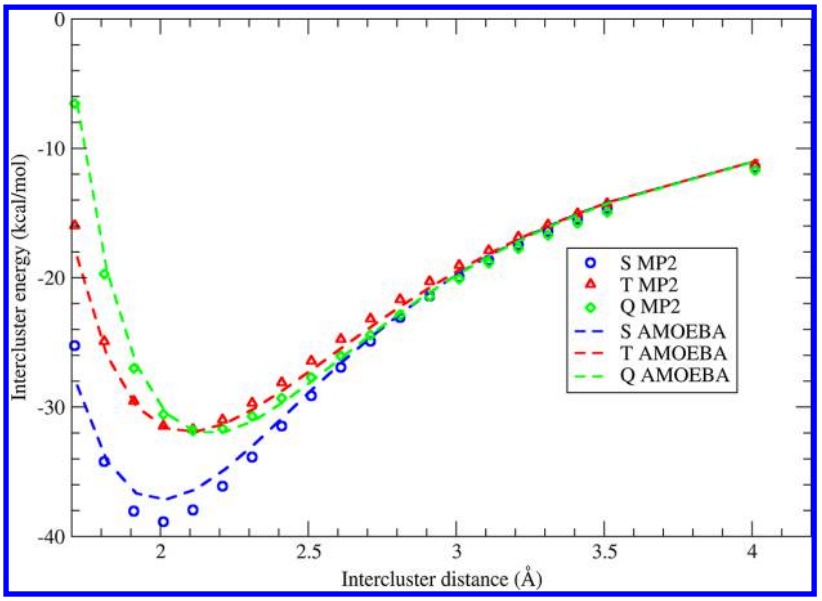

Figure 5. $[Fe(H_2O)_5]^{2+}$–H_2O dissociation profiles for the singlet, triplet, and quintet spin states along the quintet dissociation path.

Table 2. Unique Fe–O Distances (Å) for the M06-L and AMOEBA Optimized Structures of $Fe^{2+}(H_2O)_6$ at the Three Spin Multiplicities and Difference from the Shortest in Parentheses

singlet		triplet		quintet	
M06-L	AMOEBA	M06-L	AMOEBA	M06-L	AMOEBA
2.032	2.023	2.029	2.099	2.118	2.159
2.071 (0.039)	2.045 (0.022)	2.064 (0.035)	2.142 (0.043)	2.167 (0.049)	2.189 (0.030)
2.075 (0.043)	2.048 (0.025)	2.186 (0.157)	2.147 (0.048)	2.174 (0.056)	2.192 (0.033)

Table 3. Average Coordination Numbers (CN) and Fe–O Distances (Å) for the First and Second Solvation Shells of Fe^{2+} for Various Simulations

	$[Fe(H_2O)_{216}]^{2+}$, gas	$[Fe(H_2O)_{511}]^{2+}$, PBC	$[Fe(H_2O)_{781}]^{2+}$, PBC	exp.
		1st shell		
CN	6.0	6.0	6.0	6.0[66–69]
				6.1[70]
Fe–O distance	2.13	2.12	2.12	2.09[67]
				2.12[66]
				2.13[69]
				2.18[68]
				2.28[70]
		2nd shell		
CN	12.2	12.0	11.6	12.0[70]
Fe–O distance	4.25	4.25	4.27	4.30[70]
				4.43[70]
				4.51[70]

conditions (PBC). Again, three separate trajectories were propagated for this system. To assess convergence with respect to unit cell size, we also simulated a cubic box containing 781 molecules of water with an edge length of 28.643 Å subject to PBC. Key data from these various simulations are reported in Table 3.

The radial distribution functions (RDFs) for all simulations exhibited a first maximum from 2.12 to 2.13 Å, which is in good agreement with experimental measurements ranging from 2.09 to 2.18 Å,[66–69] although a substantially larger value of 2.28 Å has also been reported.[70] The present simulations suggest that this latter value may be suspect. The second solvation shell is associated with a broad peak in the RDF predicted to be between 4.25 and 4.27 Å from our AMOEBA simulations. This second maximum is again close to the experimental values ranging from 4.30 to 4.51 Å.[66–70] The average RDF computed for the simulation box containing 511 water molecules is presented in Figure 6.

Integrating the various RDFs, the first shell of hydration is predicted to include 6.0 molecules on average for all simulations, with an instantaneous value of 6 found at least 94% of the time in each trajectory; a value of 6.0 agrees with experimental observations.[66–70] Over the various simulations, we predict the second shell to be composed of 11.6–12.2 molecules on average, with an instantaneous value of 12 from 26 to 27% of the time. These results may be compared to QM/MM[74] and quantum mechanical charge field[75] molecular dynamics simulations. In the first case, RDF maxima were

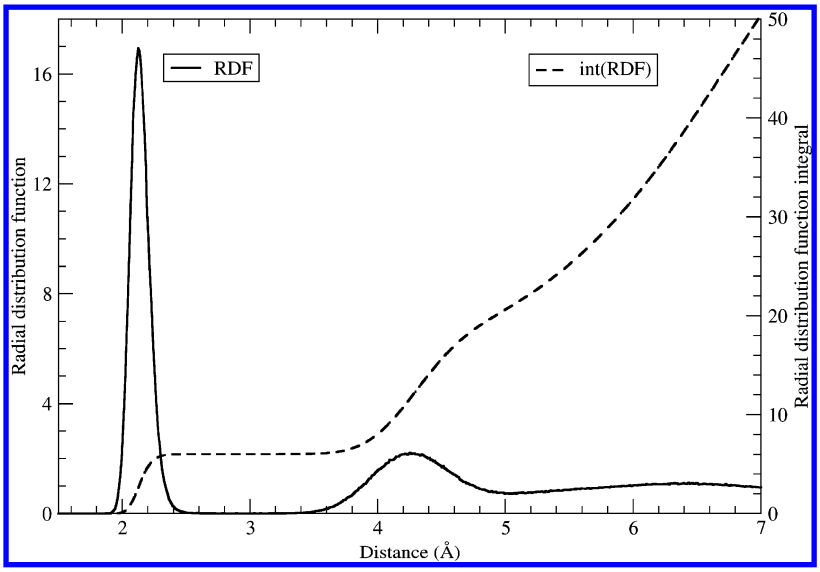

Figure 6. Radial distribution function (solid line) and integrated number density (dashed line) for water structure around Fe^{2+} in $[Fe(H_2O)_{511}]^{2+}$ with periodic boundary conditions.

predicted at 2.10 and 4.50 Å, while in the latter case, the first maximum was predicted at 2.15 Å and the second shell was found to span a distance from 3.75−5.25 Å.

During our 2 ns simulations, water molecule exchanges were observed in the first solvation shell of the cation. The event frequency was much too small to determine an average residence time of a water molecule in the first solvation shell of Fe^{2+}, but these exchanges are inconsistent with the experimentally determined residence time of ca. 220 ns.[76]

Through parametrization against $[Fe(H_2O)_5]^{2+}$−H_2O, it appears that our derived AMOEBA parameters are transferable to the bulk aqueous phase, at least within the context of structural analysis. We turn next to energetics.

IV.3. Free Energy of Hydration. As described in section II.5.2, we used the Bennett acceptance ratio[60] technique to compute the free energy changes due to perturbations between consecutive windows of a 55-trajectory growth/annihilation scheme. With a 50 ps equilibration protocol, we predict a free energy of hydration of −402.3 kcal/mol for Fe^{2+}. If we consider 200 ps for the equilibration phase, the hydration free energy thus obtained differs by 0.07 kcal/mol from this value and for each perturbation window, on average, the difference is smaller than 0.007 kcal/mol. The experimental value is −440 kcal/mol;[71] thus, the underestimation we obtain represents an error of 8.6%. A part of this difference may arise from the absence of a surface potential in our model, since Ewald summations are used with periodic boundary conditions.[77]

Given the manner in which we parametrized the ferrous ion, some underestimation of the solvation free energy was inevitable. That is, we developed force field parameters appropriate for the addition of the *last* molecule of water to the solvation shell, but the annihilation scheme appropriate for the computation of the full free energy of solvation may be regarded as summing the energetics associated with sequentially removing *each* of the first-shell water ligands. As charge transfer leads to substantial stabilization of, for instance, $Fe^{2+}(H_2O)$, and as we do not include a charge transfer term in our AMOEBA extension, the parameters appropriate for highly solvated ferrous ion are less appropriate for minimally solvated ferrous ion. To quantify this point, we may consider the binding energy of Fe^{2+} to H_2O: at the BSSE-corrected MP2 level that value is −76.6 kcal/mol at 1.95 Å, while with our current AMOEBA parametrization it is −65.3 kcal/mol at 2.01 Å. That difference is 38% of the error in our computed solvation free energy.

Thus, we deem our derived parameters appropriate for the simulation of ferrous ion in aqueous solutions represented by AMOEBA water. Future work will focus on extension to solvents and ligands interacting with iron via lone pairs on nitrogen atoms.

V. CONCLUSIONS

We extended the AMOEBA force field to all spin states of Fe^{2+} based on first-principles calculations for the bare ion and for interaction energies between $Fe^{2+}(H_2O)_5$ and H_2O. The use of a significantly hydrated cluster avoids parametrization artifacts associated with large charge transfer effects in smaller systems; in particular, localized molecular orbital energy decomposition analysis provides more physical energy partitions when computation of polarization energies is the goal.

At the ab initio level, we found all three spin states of Fe^{2+} to be well modeled by the same atomic polarizabilities and optimized damping factors. Differences in structural and energetic properties associated with singlet, triplet, and quintet spin states can be accurately modeled through optimization of vdW parameters specific to each.

We validated our extended force field against experimental data for quintet aqueous ferrous ion through molecular dynamics simulations confirming good transferability of our parameters to the bulk phase. Simulated solvent structures around the cation are in a good agreement with experiment for coordination numbers and radial distribution maxima. The free energy of solvation of Fe^{2+} is reproduced by the force field to within 8.6%. Underestimation of the solvation free energy is associated with charge transfer interactions not explicitly accounted for in the force field but is of limited importance for simulations in bulk solution, where solvation shells are expected always to be reasonably complete. We anticipate that this approach will prove fruitful for other cations having charges

of 2 or higher, although inclusion of explicit valence-bond terms in the force field may be required in some circumstances.

■ ASSOCIATED CONTENT

Supporting Information

CASPT2 single point energies associated with S, T, and Q spin multiplicities computed for selected structures of hexahydrated iron(II); relative BSSE-corrected dissociation curves, including the state-energy splittings of $[Fe(H_2O)_5]^{2+}$; and comparison of energy components obtained with LMOEDA and AMOEBA for $Fe^{2+}-(H_2O)_6$ and $Fe^{2+}(H_2O)_5-(H_2O)$ at optimized structures. This material is available free of charge via the Internet at http://pubs.acs.org.

■ AUTHOR INFORMATION

Corresponding Author

*E-mail: cramer@umn.edu; gagliard@umn.edu.

Notes

The authors declare no competing financial interest.

■ ACKNOWLEDGMENTS

Support from the National Science Foundation (CHE-1124244) is gratefully acknowledged.

■ REFERENCES

(1) Klug, A.; Schwabe, J. W. *FASEB J.* **1995**, *9*, 597−604.
(2) Kretsinger, R. H.; Nockolds, C. E. *J. Biol. Chem.* **1973**, *248*, 3313−3326.
(3) Lewit-Bentley, A.; Réty, S. *Curr. Opin. Struct. Biol.* **2000**, *10*, 637−643.
(4) Howard, J. B.; Rees, D. C. *Proc. Natl. Acad. Sci. U.S.A.* **2006**, *103*, 17088−17093.
(5) Terwilliger, N. B. *J. Exp. Biol.* **1998**, *201*, 1085−98.
(6) Meyer, J. *J. Biol. Inorg. Chem.* **2008**, *13*, 157−170.
(7) Athavale, S. S.; Petrov, A. S.; Hsiao, C.; Watkins, D.; Prickett, C. D.; Gossett, J. J.; Lie, L.; Bowman, J. C.; O'Neill, E.; Bernier, C. R.; Hud, N. V.; Wartell, R. M.; Harvey, S. C.; Williams, L. D. *PLoS ONE* **2012**, *7*, e38024.
(8) Bloch, E. D.; Queen, W. L.; Krishna, R.; Zadrozny, J. M.; Brown, C. M.; Long, J. R. *Science* **2012**, *335*, 1606−1610.
(9) Mal, P.; Schultz, D.; Beyeh, K.; Rissanen, K.; Nitschke, J. *Angew. Chem., Int. Ed.* **2008**, *47*, 8297−8301.
(10) Bilbeisi, R. A.; Clegg, J. K.; Elgrishi, N.; Hatten, X. d.; Devillard, M.; Breiner, B.; Mal, P.; Nitschke, J. R. *J. Am. Chem. Soc.* **2012**, *134*, 5110−5119.
(11) Marjolin, A.; Gourlaouen, C.; Clavaguéra, C.; Ren, P.; Wu, J.; Gresh, N.; Dognon, J.-P.; Piquemal, J.-P. *Theor. Chem. Acc.* **2012**, *131*, 1−14.
(12) Gresh, N.; Pullman, A.; Claverie, P. *Int. J. Quantum Chem.* **1985**, *28*, 757−771.
(13) Amira, S.; Spångberg, D.; Zelin, V.; Probst, M.; Hermansson, K. *J. Phys. Chem. B* **2005**, *109*, 14235−14242.
(14) Tofteberg, T.; Öhrn, A.; Karlström, G. *Chem. Phys. Lett.* **2006**, *429*, 436−439.
(15) Hagberg, D.; Bednarz, E.; Edelstein, N. M.; Gagliardi, L. *J. Am. Chem. Soc.* **2007**, *129*, 14136−14137.
(16) Xiang, J. Y.; Ponder, J. W. *J. Comput. Chem.* **2013**, *34*, 739−749.
(17) Ayed, T.; Seydou, M.; Réal, F.; Montavon, G.; Galland, N. *J. Phys. Chem. B* **2013**, *117*, 5206−5211.
(18) Helm, L.; Merbach, A. *Chem. Rev.* **2005**, *105*, 1923−1960.
(19) D'Angelo, P.; Spezia, R. *Chem.—Eur. J.* **2012**, *18*, 11162−11178.
(20) Hofer, T. S.; Pribil, A. B.; Randolf, B. R.; Rode, B. M. *Adv. Quantum Chem.* **2010**, *59*, 213−246.
(21) Warshel, A.; Kato, M.; Pisliakov, A. V. *J. Chem. Theory Comput.* **2007**, *3*, 2034−2045.
(22) Satpati, P.; Clavaguéra, C.; Ohanessian, G.; Simonson, T. *J. Phys. Chem. B* **2011**, *114*, 6749−6763.
(23) Sakharov, D. V.; Lim, C. *J. Comput. Chem.* **2009**, *30*, 191−202.
(24) Cieplak, P.; Dupradeau, F.-Y.; Duan, Y.; Wang, J. *J. Phys.: Condens. Matter* **2009**, *21*, 333102.
(25) Ren, P.; Ponder, J. W. *J. Comput. Chem.* **2002**, *23*, 1497−1506.
(26) Ren, P.; Ponder, J. W. *J. Phys. Chem. B* **2003**, *107*, 5933−5947.
(27) Ponder, J. W.; Wu, C.; Ren, P.; Pande, V. S.; Chodera, J. D.; Schnieders, M. J.; Haque, I.; Mobley, D. L.; Lambrecht, D. S.; DiStasio, R. A.; Head-Gordon, M.; Clark, G. N. I.; Johnson, M. E.; Head-Gordon, T. *J. Phys. Chem. B* **2010**, *114*, 2549−2564.
(28) Applequist, J.; Carl, J. R.; Fung, K.-K. *J. Am. Chem. Soc.* **1972**, *94*, 2952−2960.
(29) Tholé, B. *Chem. Phys.* **1981**, *59*, 341−350.
(30) van Duijnen, P. T.; Swart, M. *J. Phys. Chem. Phys. A* **1998**, *102*, 2399−2407.
(31) Swart, M.; Güell, M.; Solà, M. *Phys. Chem. Chem. Phys.* **2011**, *13*, 10449.
(32) Becke, A. D.; Edgecombe, K. E. *J. Chem. Phys.* **1990**, *92*, 5397−5403.
(33) Balabanov, N. B.; Peterson, K. A. *J. Chem. Phys.* **2005**, *123*, 064107.
(34) Clavaguéra, C.; Dognon, J. P. *Chem. Phys.* **2005**, *311*, 169−176.
(35) Réal, F.; Vallet, V.; Clavaguéra, C.; Dognon, J.-P. *Phys. Rev. A: At., Mol., Opt. Phys.* **2008**, *78*, 052502.
(36) Werner, H.-J.; Knowles, P. J.; Knizia, G.; Manby, F. R.; Schütz, M.; Celani, P.; Korona, R.; Lindh, R.; Mitrushenkov, A.; Rauhut, G.; Shamasundar, K. R.; Adler, T. B.; Amos, R. D.; Bernhardsson, A.; Berning, A.; Cooper, D. L.; Deegan, M. J. O.; Dobbyn, A. J.; Eckert, F.; Goll, E.; Hampel, C.; Hesselmann, A.; Hetzer, G.; Hrenar, T.; Jansen, G.; Köppl, C.; Liu, Y.; Lloyd, A. W.; Mata, R. A.; May, A. J.; McNicholas, S. J.; Meyer, W.; Mura, M. E.; Nicklaß, A.; O'Neil, D. P.; Palmieri, P.; Deng, D.; Pflüger, K.; Pitzer, R.; Reiher, M.; Shiozaki, T.; Stoll, H.; Stone, A. J.; Tarroni, R.; Thorsteinsson, T.; Wang, M. *MOLPRO*, Version 2010.1, a package of ab initio programs; University College Cardiff Consultants Limited: Wales, U.K., 2010.
(37) Kellö, V.; Sadlej, A. J.; Faegri, K., Jr. *Phys. Rev. A: At., Mol., Opt. Phys.* **1993**, *47*, 1715−1725.
(38) Sims, J. S.; Rumble, J.; John, R. *Phys. Rev. A: At., Mol., Opt. Phys.* **1973**, *8*, 2231−2235.
(39) Zhao, Y.; Truhlar, D. G. *J. Chem. Phys.* **2006**, *125*, 194101.
(40) Cramer, C. J.; Truhlar, D. G. *Phys. Chem. Chem. Phys.* **2009**, *11*, 10757−10816.
(41) Zhao, Y.; Truhlar, D. *Theor. Chem. Acc.* **2008**, *120*, 215−241.
(42) Dolg, M.; Wedig, U.; Stoll, H.; Preuss, H. *J. Chem. Phys.* **1987**, *86*, 866−872.
(43) Weigend, F.; Ahlrichs, R. *Phys. Chem. Chem. Phys.* **2005**, *7*, 3297−3305.
(44) Weigend, F. *Phys. Chem. Chem. Phys.* **2006**, *8*, 1057−1065.
(45) Boys, S.; Bernardi, F. *Mol. Phys.* **1970**, *19*, 553−566.
(46) Frisch, M. J.; Trucks, G. W.; Schlegel, H. B.; Scuseria, G. E.; Robb, M. A.; Cheeseman, J. R.; Scalmani, G.; Barone, V.; Mennucci, B.; Petersson, G. A.; Nakatsuji, H.; Caricato, M.; Li, X.; Hratchian, H. P.; Izmaylov, A. F.; Bloino, J.; Zheng, G.; Sonnenberg, J. L.; Hada, M.; Ehara, M.; Toyota, K.; Fukuda, R.; Hasegawa, J.; Ishida, M.; Nakajima, T.; Honda, Y.; Kitao, O.; Nakai, H.; Vreven, T.; Montgomery, J. A., Jr.; Peralta, J. E.; Ogliaro, F.; Bearpark, M.; Heyd, J. J.; Brothers, E.; Kudin, K. N.; Staroverov, V. N.; Keith, T.; Kobayashi, R.; Normand, J.; Raghavachari, K.; Rendell, A.; Burant, J. C.; Iyengar, S. S.; Tomasi, J.; Cossi, M.; Rega, N.; Millam, J. M.; Klene, M.; Knox, J. E.; Cross, J. B.; Bakken, V.; Adamo, C.; Jamarillo, J.; Gomperts, R.; Stratmann, R. E.; Yazyev, O.; Austin, A. J.; Cammi, R.; Pomelli, C.; Ochterski, J. W.; Martin, R. L.; Morokuma, K.; Zakrzewksi, V. G.; Voth, G. A.; Salvado, P.; Dannenberg, J. J.; Dapprich, S.; Daniels, A. D.; Farkas, O.; Foresman, J. B.; Ortiz, J. V.; Ciolowski, J.; Fox, D. J. Gaussian 09, Revision C.01; Gaussian Inc.: Wallingford, CT, 2009.
(47) Roos, B. O.; Lindh, R.; Malmqvist, P. A.; Veryazov, V. P.; Widmark, O. *Chem. Phys. Lett.* **2005**, *409*, 295−299.
(48) Su, P.; Li, H. *J. Chem. Phys.* **2009**, *131*, 014102−15.

(49) Chen, Y.; Li, H. *J. Phys. Chem. A* **2010**, *114*, 11719−11724.
(50) Thom, H.; Dunning, J. *J. Chem. Phys.* **1989**, *90*, 1007−1023.
(51) Gordon, M.; Schmidt, M. Advances in electronic structure theory: GAMESS a decade later. In *Theory and Applications of Computational Chemistry: The First Forty Years*; Dykstra, C., Frenking, G., Kim, K., Scuseria, G., Eds.; Elsevier: Amsterdam, 2005; pp 1167−1189.
(52) Halgren, T. A. *J. Am. Chem. Soc.* **1992**, *114*, 7827−7843.
(53) Ponder, J. W. *TINKER: Software Tools for Molecular Design*, Version 6.0; Washington University, School of Medicine: Saint Louis, MO, 2011.
(54) Beeman, D. *J. Comput. Phys.* **1976**, *20*, 130−139.
(55) Berendsen, H. J. C.; Postma, J. P. M.; van Gunsteren, W. F.; DiNola, A.; Haak, J. R. *J. Chem. Phys.* **1984**, *81*, 3684−3690.
(56) Grossfield, A.; Ren, P.; Ponder, J. W. *J. Am. Chem. Soc.* **2003**, *125*, 15671−15682.
(57) Wu, J. C.; Piquemal, J.-P.; Chaudret, R.; Reinhardt, P.; Ren, P. *J. Chem. Theory Comput.* **2010**, *6*, 2059−2070.
(58) Hagberg, D.; Karlström, G.; Roos, B. J.; Gagliardi, L. *J. Am. Chem. Soc.* **2005**, *127*, 14250−14256.
(59) Morishita, T. *J. Chem. Phys.* **2000**, *113*, 2976−2982.
(60) Bennett, C. H. *J. Comput. Phys.* **1976**, *22*, 245−268.
(61) Kohout, M. *DGrid*, Version 4.6, 2011.
(62) Stone, A. J. *The Theory of Intermolecular Forces*; Oxford University Press Inc., New York, 1996; p 37.
(63) Young, D. M. *Iterative Solution of Large Linear Systems; Computer Science and Applied Mathematics*; Academic Press: New York, 1971; Reprinted in 2003.
(64) Piquemal, J.-P.; Perera, L.; Cisneros, G. A.; Ren, P.; Pedersen, L. G.; Darden, T. A. *J. Chem. Phys.* **2006**, *125*, 054511.
(65) Zhang, J.; Yand, W.; Piquemal, J.-P.; Ren, P. *J. Chem. Theory Comput.* **2012**, *8*, 1314−1324.
(66) Ohtaki, H.; Yamaguchi, T.; Maeda, M. *Bull. Chem. Soc. Jpn.* **1976**, *49*, 701−708.
(67) Sham, T.; Hastings, J.; Perlman, M. *Chem. Phys. Lett.* **1981**, *83*, 391−396.
(68) Apted, M.; Waychunas, G.; Brown, G. *Geochim. Cosmochim. Acta* **1985**, *49*, 2081−2089.
(69) Herdman, G. J.; Neilson, G. W. *J. Phys.: Condens. Matter* **1992**, *4*, 649.
(70) Kálmán, E.; Radnai, T.; Pálinkás, G.; Hajdu, F.; Vértes, A. *Electrochim. Acta* **1988**, *33*, 1223−1228.
(71) Wagman, D. D.; Evans, W. H.; Parker, V. B.; Schumm, R. H.; Halow, I.; Bailey, S. M.; Churney, K. L.; Nuttall, R. L. *J. Phys. Chem. Ref. Data* **1982**, *11* (Supplement No. 2), 177−182.
(72) Ohtaki, H.; Radnai, T. *Chem. Rev.* **1993**, *93*, 1157−1204.
(73) Marcus, Y. *Biophys. Chem.* **1994**, *51*, 111−127.
(74) Remsungnen, T.; Rode, B. M. *J. Phys. Chem. A* **2003**, *107*, 2324−2328.
(75) Moin, S. T.; Hofer, T. S.; Pribil, A. B.; Randolf, B. R.; Rode, B. M. *Inorg. Chem.* **2010**, *49*, 5101−5106.
(76) Ducommun, Y.; Newman, K. E.; Merbach, A. E. *Inorg. Chem.* **1980**, *19*, 3696−3703.
(77) Joung, I. S.; Cheatham, T. E., III *J. Phys. Chem. B* **2008**, *112*, 9020−9041.